

Binary Black Holes: Spin Dynamics and Gravitational Recoil

Frank Herrmann, Ian Hinder, Deirdre M. Shoemaker,* and Pablo Laguna†

*Center for Gravitational Wave Physics
The Pennsylvania State University,
University Park, PA 16802*

Richard A. Matzner

*Center for Relativity and Department of Physics
The University of Texas at Austin, Austin, TX 78712*

We present a study of spinning black hole binaries focusing on the spin dynamics of the individual black holes as well as on the gravitational recoil acquired by the black hole produced by the merger. We consider two series of initial spin orientations away from the binary orbital plane. In one of the series, the spins are anti-aligned; for the second series, one of the spins points away from the binary along the line separating the black holes. We find a remarkable agreement between the spin dynamics predicted at 2nd post-Newtonian order and those from numerical relativity. For each configuration, we compute the kick of the final black hole. We use the kick estimates from the series with anti-aligned spins to fit the parameters in the Kidder kick formula, and verify that the recoil along the direction of the orbital angular momentum is $\propto \sin \theta$ and on the orbital plane $\propto \cos \theta$, with θ the angle between the spin directions and the orbital angular momentum. We also find that the black hole spins can be well estimated by evaluating the isolated horizon spin on spheres of constant coordinate radius.

Keywords: black hole physics — gravitation — gravitational waves — relativity

I. INTRODUCTION

Immediately after the discovery of the *Moving Puncture Recipe* (MPR) [1, 2], a recipe providing the ingredients to successfully evolve binary black holes (BBHs), the numerical relativity efforts focused on studying the gravitational recoil or kick acquired by the black hole (BH) produced in the merger [3, 4, 5]. The main driving force behind these studies has been the astrophysical implications of these kicks on the supermassive black holes (SMBHs) at the centers of galaxies [6, 7]. Specifically, a detailed understanding of these kicks is vital to explain the demographics, growth and merger rates of SMBHs [8, 9], as well as their absence in dwarf galaxies and stellar clusters [10, 11].

When viewed in terms of modes of the gravitational radiation emitted by the binary, kicks arise from the overlap of those modes [12, 13]. A non-vanishing overlap will be produced if the BHs in the binary have un-equal masses and/or are spinning with non-trivial relative orientations. For kicks from non-spinning BBHs, the most comprehensive numerical relativity study [5] showed that one can parameterize the magnitude of the kick velocity as

$$V = A \frac{q^2 (1-q)}{(1+q)^5} \left[1 + B \frac{q}{(1+q)^2} \right], \quad (1)$$

with $A = 1.2 \times 10^4 \text{ km s}^{-1}$, $B = -0.93$ and $q = M_1/M_2$. This parameterization was motivated by the scalings originally introduced by Fitchett [14, 15]. From Eq. (1), the maximum kick has a magnitude of 175 km s^{-1} and occurs at $q = 0.36$ or symmetrized reduced mass $\eta = M_1 M_2 / M^2 = 0.195$, with $M = M_1 + M_2$ the total mass of the binary. Other mass parameters that will be used are $\delta M \equiv M_1 - M_2$ and $\mu \equiv M_1 M_2 / M$. When compared to the escape velocities of galactic structures, the kicks from non-spinning and un-equal mass binaries are modest. They are not high enough to eject the BH from its host galaxy [11].

The next frontier was to investigate kicks in which the emission of linear momentum was due to the spin of the BHs. The first study of this kind [13] produced kick velocities of $V = 475 \text{ km s}^{-1} a/M$ for BHs with opposite and equal magnitude spins parallel to the orbital angular momentum. Similar studies followed soon after [16, 17] that produced complementary results. The kick velocities of $\sim 500 \text{ km s}^{-1}$ obtained from these configurations could in principle explain the absence of massive BHs in dwarf ellipticals [11]. Motivated by post-Newtonian (PN) results [18],

*Also at Department of Physics and Institute for Gravitation and the Cosmos

†Also at Departments of Astronomy & Astrophysics, Physics and Institute for Gravitation and the Cosmos

it was immediately realized that the orientation of the BHs' spins has a profound effect on the kick that the final BH receives. Gonzalez et al. [19] carried out the first simulations in which the spins of the BHs are initially anti-aligned in the orbital plane and found that kick velocities of at least 2500 km s^{-1} are possible. Similar studies [20] suggest that the kick could be scaled to reach a maximum of $\sim 4000 \text{ km s}^{-1}$.

As more studies of gravitational recoil continued to emerge, generalizations of the phenomenological kick formula Eq. (1) to include spins have been introduced [20, 21, 22], all motivated by the structure of the formula for the rate of linear momentum radiated, a formula first derived by Kidder [18]. The terms involving spin-orbit effects in this formula read

$$\frac{d\mathbf{P}}{dt} = -\frac{8}{15} \frac{M^3}{r^5} \frac{q^2}{(1+q)^4} \left\{ 4\dot{r}(\mathbf{v} \times \boldsymbol{\Sigma}) - 2v^2(\mathbf{n} \times \boldsymbol{\Sigma}) - (\mathbf{n} \times \mathbf{v})[3\dot{r}(n\Sigma) + 2(v\Sigma)] \right\}, \quad (2)$$

where (ab) denotes the vector dot product, i.e. $(ab) = \mathbf{a} \cdot \mathbf{b}$. We are following as closely as possible the notation in Ref. [23] and introduce the spin variables

$$\begin{aligned} \mathbf{S} &\equiv \mathbf{S}_1 + \mathbf{S}_2 \\ \boldsymbol{\Sigma} &\equiv M \left(\frac{\mathbf{S}_2}{M_2} - \frac{\mathbf{S}_1}{M_1} \right), \end{aligned}$$

where the vector \mathbf{x} denotes the relative position vector of M_2 with respect to M_1 , with $r = |\mathbf{x}|$, $\mathbf{v} = d\mathbf{x}/dt$, $\mathbf{n} = \mathbf{x}/r$ and $\mathbf{L}_N \equiv \mu \mathbf{x} \times \mathbf{v}$, the Newtonian angular momentum. We also introduce a flat-space orthonormal rotating triad $\{\mathbf{n}, \mathbf{k}, \mathbf{l}\}$ such that $\mathbf{k} = \mathbf{l} \times \mathbf{n}$ with $\mathbf{l} = \mathbf{L}_N/|\mathbf{L}_N|$ and hence \mathbf{l} is perpendicular to the orbital plane.

With these definitions, Eq. (2) has the following structure:

$$\frac{d\mathbf{P}}{dt} = [\dots](\mathbf{k} \times \boldsymbol{\Sigma}) + [\dots](\mathbf{n} \times \boldsymbol{\Sigma}) + \left\{ [\dots](k\Sigma) + [\dots](n\Sigma) \right\} \mathbf{l}, \quad (3)$$

or equivalently

$$\frac{d\mathbf{P}}{dt} = \left\{ [\dots]\mathbf{k} + [\dots]\mathbf{n} \right\} (l\Sigma) + \left\{ [\dots](k\Sigma) + [\dots](n\Sigma) \right\} \mathbf{l}, \quad (4)$$

where we only show the explicit dependence on $\boldsymbol{\Sigma}$ relative to the orthonormal tetrad. Given the form of Eq. (4), we propose the following parameterization of the contribution of the spins to the gravitational recoil:

$$\mathbf{V} = \frac{\Sigma}{M^2} \frac{q^2}{(1+q)^4} \left\{ [H_k \mathbf{k} + H_n \mathbf{n}](l\sigma) + [K_k(k\sigma) + K_n(n\sigma)]\mathbf{l} \right\}, \quad (5)$$

where $\sigma = \boldsymbol{\Sigma}/|\boldsymbol{\Sigma}|$. We will refer to Eq. (5) as the Kidder kick formula.¹ The parameters H_k , H_n , K_k and K_n in Eq. (5) are to be determined from numerical simulations. A fundamental aspect of the validity of this formula is the dependence of the kick velocity on the cosine angles $(l\sigma)$, $(k\sigma)$ and $(n\sigma)$. Spin precession will force these angles to evolve in time. Thus, one is faced with the task of measuring the *entrance* angles. These are the angle values when the binary reaches the ‘‘last’’ orbit or plunge, namely the time that signals the beginning of the phase when the bulk of the kick gets accumulated. An identification of the *entrance* angles would allow one to determine the H_k , H_n , K_k and K_n parameters in Eq. (5) from numerical simulations.

The work in this paper is aimed at exploring the parameter space of spinning BBHs with focus on the dynamics of the individual spins and the kick that the final BH receives. We consider two series of equal mass BHs (i.e. $\delta M = 0$). In one series, called the *B-series*, the BHs initially have equal spin magnitudes and anti-aligned directions. That is, $\mathbf{S} = 0$ and $\boldsymbol{\Sigma} = 4\mathbf{S}_2 = -4\mathbf{S}_1$. The elements of this series are obtained by changing the orientation of $\boldsymbol{\Sigma}$ relative to the unit vector \mathbf{l} . In the second series, called the *S-series*, we also keep the spin magnitudes constant. What changes in this series is the relative alignment of the spins. For each run in both series, we monitor the precession dynamics of the individual spins and compare them with PN predictions. We find a remarkable agreement with 2PN results: the 2PN dynamics closely match those from numerical relativity up to the point when a common apparent horizon (AH) is formed. For all models, we compute the gravitational recoil on the final BH. We use the kick estimates from the *B-series* to find parameters in the Kidder kick formula and also verify the angular dependence in \mathbf{V} that this formula

¹ There are several versions of parameterized kick formulas. Since all are motivated by Kidder's seminal work [18], we will generically call them *Kidder kick formulae*.

implies. As numerical relativity efforts explore different regions of the parameter space, the values of the parameters in Eq. (5) will be improved or validated. A phenomenological formula of this kind is of great value for astrophysical studies such as those explaining the population of SMBHs.

The paper is organized as follows: In Sec. II, we use a multipole analysis to demonstrate the dependence of the kicks on the spin orientations as given by the Kidder kick formula. In Sec. III, we summarize our computational infrastructure. A detailed description of the two series of initial data configurations is given in Sec. IV. The analysis of the BH spin dynamics is presented in Sec. V. Kick results, including the fit to the Kidder kick formula, are given in Sec. VI. We end with conclusions in Sec. VII.

II. KICKS AND ENTRANCE ANGLES

To gain further understanding of the Kidder kick formula, we present an analysis based on the multipole formulas of Refs. [12, 18], in which the rate of radiated linear momentum is estimated, to lowest order, as an interference of the mass and spin quadrupoles. Excluding non-spin terms, this formula reads

$$\frac{dP^i}{dt} = \frac{16}{45}\epsilon^{ijk}I_{jl}^{(3)}H_{kl}^{(3)} + \frac{4}{63}H_{ijk}^{(4)}H_{jk}^{(3)} + \frac{1}{126}\epsilon^{ijk}I_{jlm}^{(4)}H_{klm}^{(4)}. \quad (6)$$

Here I_{ij} and I_{ijk} are respectively the mass quadrupole and octupole. Similarly, H_{ij} and H_{ijk} are the spin quadrupole and octupole, respectively. In Eq. (6), a super-index $^{(n)}$ denotes an n th-time derivative.

In previous work [13], we used the first term (interference between the mass and the spin quadrupoles) to estimate the kick from quasi-circular inspiral to merger by integrating Eq. (6). This term is periodic, with period equal to the orbital period, so the kick is dominated by the “last” half orbit in the inspiral. The estimate is computed by integrating over a close-in half orbit (as in Section I, the result depends on the magnitude and direction of the spins with respect to the orbital angular momentum $\mathbf{L} = L\mathbf{l}$), and absorbing the resulting error as a normalization constant, where the constant is fixed by comparing estimate to numerics for *one* configuration. We take the same approach here.

Note that the second term in Eq. (6) will be quadratic in the spin, but the spin multipoles have one extra factor $(\mathbf{S}_{1,2}/M_{1,2})/d$ (where d is the “last orbit separation”, and of order several M) that suppresses the radiation from this term by the same factor compared to the first term. While this term’s contribution may become important in the future, for the moderate spin values we (and others) are currently considering, we do not expect significant *nonlinear* dependence. The third term vanishes (the mass octupole vanishes) for equal mass circular orbits as appropriate to our computational quasi-circular inspiral, so the equation in our current context is just the first term.

For the purpose of investigating the *entrance* angles, we consider a binary system consisting of equal mass BHs in circular orbit initially confined to the xy plane. The orbit is initially oriented so that the BHs are located on the x -axis, the BH₁ on the positive x -axis and BH₂ on the negative x -axis. We discuss first the case in which only the BH₁ is spinning. We parameterize the orientation of the spin using the usual (fixed frame) polar and axial angles θ and φ . Thus we have $S_{1x} = S_1 \sin\theta \cos\varphi$, $S_{1y} = S_1 \sin\theta \sin\varphi$ and $S_{1z} = S_1 \cos\theta$.

The calculation of the mass quadrupole is straightforward, see e.g. [13]; the spin quadrupole can be most easily calculated by imagining a spin dipole (charges $\pm M_1/2$, separation S_1/M_1) and conceptually taking the limit at the end. The spin enters only linearly in the spin quadrupole H_{kl} . The structure is different for spin components in different directions, and we can compute them independently for the different components. The nonzero components are:

For S_{1x} :

$$\begin{aligned} {}^{(x)}H_{xx}^{(3)} &= \frac{1}{3} d S_{1x} \omega^3 \sin(\omega t) \\ {}^{(x)}H_{yx}^{(3)} &= -\frac{1}{4} d S_{1x} \omega^3 \cos(\omega t) \\ {}^{(x)}H_{yy}^{(3)} &= -\frac{1}{6} d S_{1x} \omega^3 \sin(\omega t) \\ {}^{(x)}H_{zz}^{(3)} &= -\frac{1}{6} d S_{1x} \omega^3 \sin(\omega t); \end{aligned} \quad (7)$$

For S_{1y} :

$$\begin{aligned}
{}^{(y)}H_{xx}^{(3)} &= \frac{1}{6} dS_{1y} \omega^3 \cos(\omega t) \\
{}^{(y)}H_{yx}^{(3)} &= \frac{1}{4} dS_{1y} \omega^3 \sin(\omega t) \\
{}^{(y)}H_{yy}^{(3)} &= -\frac{1}{3} dS_{1y} \omega^3 \sin(\omega t) \\
{}^{(y)}H_{zz}^{(3)} &= \frac{1}{6} dS_{1y} \omega^3 \cos(\omega t);
\end{aligned} \tag{8}$$

For S_{1z} :

$$\begin{aligned}
{}^{(z)}H_{xz}^{(3)} &= \frac{1}{2} dS_{1z} \omega^3 \sin(\omega t) \\
{}^{(z)}H_{yz}^{(3)} &= -\frac{1}{2} dS_{1z} \omega^3 \cos(\omega t).
\end{aligned} \tag{9}$$

The spin quadrupole for arbitrary spin direction is the sum of the S_{1x}, S_{1y}, S_{1z} terms. In deriving these expressions, we assume that spins, which are parallel transported in the evolution, remain constant in Cartesian coordinates. This approximation is adequate for the level of accuracy of these estimates. The radiated linear momentum equation Eq. (6) is then explicitly:

$$\begin{aligned}
\frac{dP^x}{dt} &= \frac{8}{45} M^2 d^3 \omega^6 S_{1z} \sin(\omega t) \\
\frac{dP^y}{dt} &= -\frac{8}{45} M^2 d^3 \omega^6 S_{1z} \cos(\omega t) \\
\frac{dP^z}{dt} &= -\frac{16}{45} M^2 d^3 \omega^6 [S_{1x} \cos(\omega t) - S_{1y} \sin(\omega t)].
\end{aligned} \tag{10}$$

The in-plane component of the force rotates with the orbit; the out of plane component oscillates at the frequency of the orbit.

If there is a spin on the second hole, the forms are the same as Eqs. (10), but the angle ωt is replaced by $\omega t + \pi$. This replacement has the effect of introducing a global minus sign into the spin quadrupole for the spin on the hole initially located on the negative x -axis. This means that the kick estimate is doubled if the second spin is equal and opposite, but we estimate zero kick if the spins are equal and parallel. For generic second spin, as in our *S-series*, one simply subtracts the components in Eqs. (10) for this second spin S_2 from those for the first.

We concentrate our attention on the *B-series*. As we shall see later, this is the series for which we are going to be able to verify, from our simulations, the dependence of the Kidder kick formula on the *entrance* angles. In the *B-series*, the spins are fixed magnitude. Hence, the Eqs. (10), including the contributions from both spins, read:

$$\begin{aligned}
\frac{dP^x}{dt} &= \frac{16}{45} M^2 d^3 \omega^6 S_1 \cos \theta \sin(\omega t) \\
\frac{dP^y}{dt} &= -\frac{16}{45} M^2 d^3 \omega^6 S_1 \cos \theta \cos(\omega t) \\
\frac{dP^z}{dt} &= -\frac{32}{45} M^2 d^3 \omega^6 S_1 \sin \theta \cos(\omega t + \varphi).
\end{aligned} \tag{11}$$

Eqs. (11) predict a z -kick $V^z \propto \sin \theta$ and kicks $\propto \cos \theta$ in the orbital plane. Notice also the dependence of the z -kick on the entry angle $(\omega t + \varphi)$, demonstrating the fact that the net z -kick can vanish for carefully chosen entry angle. For the circular orbits treated here, dP^z/dt in Eqs. (11) identifies the quantities K_k and K_n in the Kidder kick formula, Eq. (5), as equal. We will compare the predictions of Eqs. (11) on the scaling of the kicks with the angle θ in Sec. VI.

III. COMPUTATIONAL METHODOLOGY

We follow the MPR to evolve the BBH configurations. Briefly, the MPR builds upon the BSSN system of evolution equations [24, 25, 26], models BHs with “punctures” [27] and uses dynamic gauge conditions [1, 2] designed to allow these punctures to move. The explicit form of the evolution equations for the lapse and shift gauge quantities are the “covariant” form of the “1+log” slicing [28] $(\partial_t - \beta^i \partial_i) \alpha = -2\alpha K$ and a modified gamma-freezing condition [29, 30]

for the shift: $\partial_t \beta^i = B^i$, $B^i = \partial_t \tilde{\Gamma}^i - \xi \partial_t \beta^i - \beta^j \partial_j \tilde{\Gamma}^i$, where K is the trace of the extrinsic curvature, $\tilde{\Gamma}^i$ the trace of the conformal connection and $\xi = 2$ a free, dissipative parameter. The importance of these gauge conditions is twofold: First, they avoid the need of excising the BH singularity from the computational domain since they effectively halt the evolution (i.e. lapse function α vanishes) near the BH singularity [31]. Second, they allow for movement of the BH or *puncture* through the computational domain while freezing the evolution inside of the BH horizon. See Ref. [32] for a detailed description and analysis of the MPR.

Our source code was produced by the `Kranc` code generation package [33] and uses the `Cactus` infrastructure [34] for parallelization and `Carpet` [35] for mesh refinement. The code uses fourth order accurate finite differencing (centered for all non-advection and a lop-sided stencil for the advection terms) and a fourth order Runge-Kutta temporal updating scheme with Courant factor of 0.5. The initial data code was developed by Ansorg et al. [36]. The initial free parameters (e.g. specifying angular momentum, spins, masses, separations) are chosen according to the effective potential method [37, 38] or using PN parameters [19, 39]. These methods both yield BBH initial data sets representing BBHs in quasi-circular orbit [32].

The computational grids consist of a nested set of 10 refinement levels, with the finest mesh having resolution $h = M/35.2$. This resolution translates into a resolution of about $h = m/14$, with respect to the bare mass, m , of the punctures according to Tables I and II. The minimal resolution found to be adequate for spinning cases according to Campanelli et al. [39] is $h < M/30$. The grid sizes in our $h = M/35.2$ simulations are: the 4 finest refinement levels have 44^3 grid-points plus 6 coarser refinement levels of 88^3 . All grids are initially cubical. During the evolution, the shape and number of grid-points per refinement level vary due to adaptivity. The coarsest mesh is kept fixed and extends to $640M$ from the origin in each direction. Because the simulations in this work are very similar (regarding mesh setups, grid sizes and refinement scales) to those in our previous work [13], the convergence and errors estimates in the present study are comparable.

In order to study the spin dynamics of the BHs, we need infrastructure to compute the individual spins of the BHs. The isolated horizon formalism [40, 41, 42] provides a definition associated with a Killing vector of the spacetime of the spin of a single BH:

$$S_\varphi = \frac{1}{8\pi} \oint_{AH} \varphi^i n^j K_{ij} dS \quad (12)$$

where φ^i is a Killing vector on the AH surface, K_{ij} is the extrinsic curvature of the 3D-slice and n^i is the outward pointing unit normal vector to the AH. The direction of the spin is given by the Killing vector φ^i . To facilitate finding the spin direction, Campanelli et al. [43] introduced the usage of the flat space coordinate rotational Killing vectors

$$\begin{aligned} \varphi_x^i &= (0, -\hat{z}, \hat{y}) \\ \varphi_y^i &= (\hat{z}, 0, -\hat{x}) \\ \varphi_z^i &= (-\hat{y}, \hat{x}, 0), \end{aligned}$$

where the coordinates $(\hat{x}, \hat{y}, \hat{z})$ are relative to the position of the BH. The spin is then given by $\mathbf{S} = (S_x, S_y, S_z)$, where each component is obtained, in the fixed $\{x, y, z\}$ coordinate system, by evaluating Eq. (12) with each of the coordinate rotational Killing vectors. There is an excellent agreement between the approximate spin this method yields and the one using the Killing vector φ^i (when one exists) [43]. There are efficient AH finders [44] available; however, they impose a non-negligible overhead in the simulations. To gain efficiency, we relax the condition that the integral in Eq. (12) has to be evaluated at the AH and choose a coordinate sphere around the puncture. The radius of the sphere is chosen sufficiently small, that the sphere is contained within the BH's horizon.

Fig. 1 shows a comparison of the S_x component between the values using the AH surface and three different coordinate spheres of radius r for the S-90 model (see Table II) BBH evolution. There is good agreement into the merger regime. The vertical line in Fig. 1 and subsequent figures shows the first time a common AH is found. After that time, no individual apparent horizons exist and the spheres centered on the punctures track different and meaningless values of S_x .

IV. INITIAL DATA AND RADIATED QUANTITIES

We consider two series of equal mass BHs (i.e. $\delta M = 0$). In both series, initially the BHs have the same spin magnitude $S_1/M_1^2 = S_2/M_2^2 = 0.6$. The initial orientation of the BH's spin is in the xz -plane. We use the polar angle θ_1 : the angle between the z -axis and the direction of \mathbf{S}_1 in the xz -plane. The BH₂ is treated similarly. We take the convention that positive (negative) θ angles are measured (counter-) clockwise in the xz -plane. In the series referred to as *B-series*, the BH's are anti-aligned, i.e. $\theta \equiv \theta_2 = \theta_1 - 180^\circ$, so $\mathbf{S}_1 = -\mathbf{S}_2$. That is, $\mathbf{S} = 0$ and $\boldsymbol{\Sigma} = 4\mathbf{S}_2 = -4\mathbf{S}_1$.

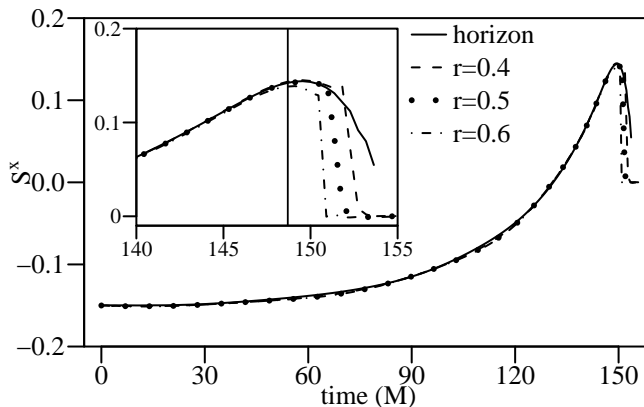


FIG. 1: Comparison of S^x computed on the horizon and from spheres with radius r for a BBH evolution (S-90 model, see Table II). The vertical line (here and in subsequent Figures) shows the first time a common AH is found.

| model | $x[M]$ | $p_y[M]$ | $V[\text{km s}^{-1}]$ | $J_{\text{rad}}[\% L_o^z]$ | $E_{\text{rad}}[\% M]$ | $T_{\text{max}}[M]$ |
|-------|--------|----------|-----------------------|----------------------------|------------------------|---------------------|
| B-20 | 2.986 | 0.138 | 427 | 24 | 3.3 | 109.1 |
| B-30 | 2.990 | 0.138 | 544 | 24 | 3.3 | 109.1 |
| B-50 | 3.000 | 0.137 | 761 | 25 | 3.4 | 108.6 |
| B-70 | 3.009 | 0.137 | 908 | 25 | 3.4 | 108.6 |
| B-80 | 3.012 | 0.137 | 945 | 25 | 3.4 | 108.4 |
| B-90 | 3.013 | 0.137 | 963 | 25 | 3.4 | 108.4 |

TABLE I: *B-series*: Initial data parameters for the *B-series*. The models in this series are labeled as B- θ , where the angle $\theta \equiv \theta_2 = \theta_1 - 180^\circ$ ($\theta = 0^\circ$ corresponds to spins parallel and anti-parallel to the orbital angular momentum). The punctures have bare masses $m_{1,2} = 0.395$, are located on the x -axis at $\mp x$ and have initial momentum $\mp p_y$ in the y -direction. Results listed are the magnitude of the recoil velocity V , the radiated angular momentum J_{rad}^z in % of the initial orbital angular momentum L_o^z , the energy radiated E_{rad} , and the time T_{max} which is an estimate of the merger time derived from the time it takes in each simulation to reach the maximum amplitude in Ψ_4 .

The elements in this series are obtained by changing θ . In the *S-series*, we initially orient \mathbf{S}_1 to $\theta_1 = 270^\circ = -90^\circ$ and vary $\theta \equiv \theta_2$.

We chose orbital parameters (i.e. bare masses, separation and momentum) in the *B-series* by minimizing the effective binding energy [38, 45], while for the *S-series* we used PN parameters [19, 39]. Initially, BH₁ is located at position $(-x/M, 0, 0)$ and has linear momentum $(0, -p_y/M, 0)$. Similarly, BH₂ is at position $(x/M, 0, 0)$ with linear momentum $(0, p_y/M, 0)$. It turns out that the bare puncture masses for both series are roughly constant, $m_1 = m_2 \approx 0.395 M$ to the 3rd digit of precision. The slight changes are needed to keep the irreducible masses $M_1 = M_2 = 0.5 M$. As mentioned above, the spins in both BHs are initially in the xz -plane; that is, $(S_{1,2}^x/M^2, 0, S_{1,2}^z/M^2)$, where $S_{1,2}^x = S_{1,2} \sin \theta_{1,2}$ and $S_{1,2}^z = S_{1,2} \cos \theta_{1,2}$ with $S_{1,2} = 0.15 M^2$.

Table I lists the relevant initial data parameters for the *B-series*, while Table II gives the parameters for the *S-series*. In addition to the initial data parameters, the tables also report the radiated angular momentum J_{rad}^z in % of the initial orbital angular momentum, L_o^z , as well as a time estimate of the common AH formation. We use the maximum in Ψ_4 shifted by the extraction radius and an additional $10 M$ as an indicator for the merger time T_{max} . We have found that this measure is accurate to a few M . For the *B-series*, the spin of the final BH is $J/M^2 = 0.62$ for all models. Constant in both series is the total ADM mass, $E_{\text{ADM}} \approx 0.985 M$. While the runs B-90 and S-90 have the same spin configurations, i.e. spins pointing along the x -axis only, the radiated energy and angular momentum are different because they differ in initial separation and angular momentum. The radiated quantities were extracted at $r = 40 M$. For a number of models, we have carried out simulations at lower resolution ($M/32$) and measured at detector radii $r/M = \{30, 40, 50, 60, 80\}$. Based on the variations observed in the measured quantities (energy, angular momentum and kicks), we estimate the reported numbers to be accurate to about 15%.

| model | $m_{1,2}[M]$ | $p_y[M]$ | $V[\text{km s}^{-1}]$ | $J_{\text{rad}}[\% L_{\text{o}}^z]$ | $E_{\text{rad}}[\% M]$ | $J_{\text{final}}^z[M^2]$ | $T_{\text{max}}[M]$ |
|-------|--------------|----------|-----------------------|-------------------------------------|------------------------|---------------------------|---------------------|
| S-0 | 0.396 | 0.132 | 854 | 34 | 4.6 | 0.68 | 192.3 |
| S-15 | 0.396 | 0.132 | 1401 | 33 | 4.4 | 0.68 | 189.5 |
| S-30 | 0.396 | 0.132 | 2000 | 33 | 4.4 | 0.67 | 184.1 |
| S-45 | 0.396 | 0.133 | 2030 | 32 | 4.3 | 0.66 | 177.3 |
| S-60 | 0.395 | 0.134 | 1218 | 30 | 4.0 | 0.65 | 168.6 |
| S-75 | 0.395 | 0.135 | 230 | 28 | 3.7 | 0.64 | 159.1 |
| S-90 | 0.395 | 0.137 | 1462 | 26 | 3.4 | 0.62 | 148.6 |
| S-105 | 0.395 | 0.138 | 1979 | 25 | 3.3 | 0.60 | 138.6 |
| S-120 | 0.395 | 0.139 | 1787 | 24 | 3.2 | 0.58 | 130.5 |
| S-135 | 0.395 | 0.140 | 1234 | 23 | 3.0 | 0.56 | 124.1 |
| S-150 | 0.395 | 0.141 | 689 | 21 | 2.9 | 0.55 | 119.5 |
| S-165 | 0.395 | 0.141 | 335 | 21 | 2.8 | 0.55 | 117.7 |
| S-180 | 0.395 | 0.141 | 188 | 20 | 2.8 | 0.55 | 117.7 |
| S-195 | 0.395 | 0.141 | 157 | 20 | 2.8 | 0.55 | 120.5 |
| S-210 | 0.395 | 0.141 | 173 | 22 | 3.0 | 0.56 | 125.5 |
| S-225 | 0.395 | 0.140 | 223 | 22 | 3.2 | 0.57 | 132.7 |
| S-240 | 0.395 | 0.139 | 268 | 23 | 3.4 | 0.59 | 141.4 |
| S-285 | 0.395 | 0.135 | 253 | 26 | 3.9 | 0.65 | 174.1 |
| S-300 | 0.396 | 0.134 | 406 | 29 | 4.2 | 0.66 | 181.8 |
| S-315 | 0.396 | 0.133 | 399 | 31 | 4.5 | 0.67 | 187.7 |
| S-330 | 0.396 | 0.132 | 354 | 32 | 4.6 | 0.68 | 191.8 |
| S-345 | 0.396 | 0.132 | 459 | 33 | 4.6 | 0.68 | 193.2 |

TABLE II: The *S-series*. For all cases, initially the BH₁ is located along the x -axis at $x = -3.1 M$, has momentum pointing along the y -direction with value $-p_y$, and has spin $\mathbf{S}_1 = (-0.15/M^2, 0, 0)$, thus $\theta_1 = -90^\circ$ and $\varphi_1 = -180^\circ$. BH₂ is located also along the x -axis but at $x = 3.1 M$ with momentum p_y . In these runs, labeled S- θ , the angle θ gives the angle in the xz -plane that the spin of BH₂ makes with respect to the z -axis. Results listed are the magnitude of the recoil velocity V , the radiated angular momentum J_{rad}^z in % of the initial orbital angular momentum L_{o}^z , the energy radiated E_{rad} , the spin of the final BH J_{final}^z along the z -axis, and the time T_{max} which is an estimate of the merger time derived from the time it takes in each simulation to reach the maximum amplitude in Ψ_4 .

V. SPIN DYNAMICS

In the present work, we are interested investigating the degree to which the spin dynamics described by PN equations agrees with that from numerical relativity. Following Ref. [46], the precession equation of BH₁ in the binary with mass M_1 , spin \mathbf{S}_1 , position \mathbf{x}_1 and velocity \mathbf{v}_1 is given by

$$\frac{d\mathbf{S}_1}{dt} = \boldsymbol{\Omega}_1 \times \mathbf{S}_1; \quad (13)$$

which implies that BH₁ precesses around the vector $\boldsymbol{\Omega}_1$ with rate $|\boldsymbol{\Omega}_1|$. The precession angular frequency vector $\boldsymbol{\Omega}_1$ is given to 2PN by

$$\begin{aligned} \boldsymbol{\Omega}_1 = & \frac{M_2}{r^2} \left[\frac{3}{2} \mathbf{n}_{12} \times \mathbf{v}_1 - 2 \mathbf{n}_{12} \times \mathbf{v}_2 \right] \\ & + \frac{M_2}{r^2} \left[\mathbf{n}_{12} \times \mathbf{v}_1 \left(-\frac{9}{4} (n_{12} v_2)^2 + \frac{1}{8} v_1^2 - (v_1 v_2) + v_2^2 + \frac{7}{2} \frac{M_1}{r} - \frac{1}{2} \frac{M_2}{r} \right) \right. \\ & \quad + \mathbf{n}_{12} \times \mathbf{v}_2 \left(3 (n_{12} v_2)^2 + 2 (v_1 v_2) - 2 v_2^2 + \frac{M_1}{r} + \frac{9}{2} \frac{M_2}{r} \right) \\ & \quad \left. + \mathbf{v}_1 \times \mathbf{v}_2 \left(3 (n_{12} v_1) - \frac{7}{2} (n_{12} v_2) \right) \right], \quad (14) \end{aligned}$$

with $\mathbf{x} = \mathbf{x}_1 - \mathbf{x}_2$, $r = |\mathbf{x}|$ and $\mathbf{n}_{12} = \mathbf{x}/r$. The expressions for the companion BH₂ are obtained by switching $1 \leftrightarrow 2$ in Eqs. (13-14). In Eq. (14), the first term in square brackets represents the 1PN contribution. For comparison, we also

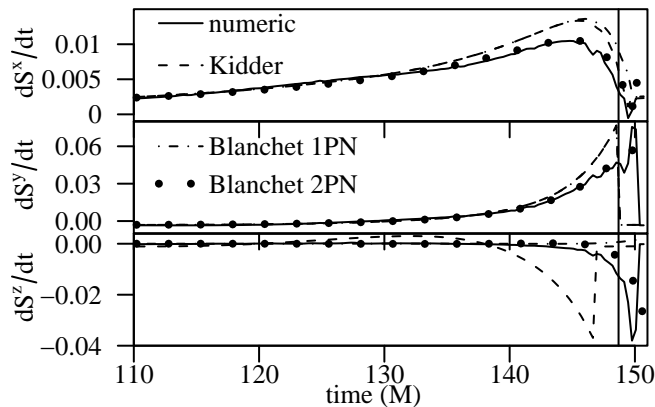


FIG. 2: Comparison of $d\mathbf{S}_1/dt$ computed from the numerical evolution directly and by using PN formulas for the S-90 run. *Kidder* describes the dynamics using precession angular frequency given by Eq. (15). *Blanchet 1PN* denotes the dynamics with Ω_1 given by the first term in Eq. (14); *Blanchet 2PN* denotes the case in which the entire expression in Eq. (14) is used. The vertical line around $t = 149M$ indicates the formation of a common apparent horizon.

show the precession angular frequency from Kidder [18], in which the terms $\propto \mathbf{L}_N$ (corresponding to the first line in Eq. (14)) are accurate to 1PN but the expression also contains spin-spin terms:

$$\Omega_1 = \frac{1}{r^3} \left[\mathbf{L}_N \left(2 + \frac{3}{2} \frac{M_2}{M_1} \right) - \mathbf{S}_2 + 3(n_{12}S_2)\mathbf{n}_{12} \right], \quad (15)$$

where $\mathbf{L}_N = \mu \mathbf{x} \times \mathbf{v}_{12}$ denotes the Newtonian angular momentum. Here again one obtains the expression for BH_2 by switching $1 \leftrightarrow 2$.

Fig. 2 shows the time evolution of $d\mathbf{S}_1/dt$ computed in four different ways for the S-90 run (the spins are equal magnitude and anti-aligned in the xy -plane). The time evolution of $d\mathbf{S}_2/dt$ is equal and opposite in this case. Solid lines, labeled *numeric*, represent the numerical relativity solutions. The values of $d\mathbf{S}_1/dt$ are obtained by constructing each BH spin as described in Sec. III, followed by finite differences to approximate the time derivative. A long dashed line, labeled *Kidder*, denotes $d\mathbf{S}_1/dt$ computed using the precession angular frequency Eq. (15). The dotted line, labeled *Blanchet 1PN*, represents the result from using only the 1PN contribution in the precession angular frequency Eq. (14); that is, it corresponds to Kidder's precession without the inclusion of spin-spin interactions. Finally, the dashed-dotted line, labeled *Blanchet 2PN*, depicts the evolution of $d\mathbf{S}_1/dt$ using the entire expression in Eq. (14). In the construction of the PN precession angular frequencies, we use the positions and velocities of the punctures from the numerical simulations. The vertical lines in Fig. 2 denote the time at which a common AH is formed.

It is remarkable how accurately the 2PN approximations of $d\mathbf{S}_1/dt$ track the numerical result deep into the merger regime, close to the formation of a common AH. Comparisons beyond the time when a common AH forms are not very meaningful since the individual trapped surfaces lose their horizon interpretation and our spin measure breaks down (see Sec. III). Also interesting is that the spin-spin terms in Kidder's expression make only a small contribution to dS^x/dt and dS^y/dt , as can be seen from the similarities of the Kidder and Blanchet 1PN lines. On the other hand, the spin-spin are responsible for the differences between the Kidder and Blanchet 1PN values of dS^z/dt near the mergers, as one can observe in the bottom panel of Fig. 2. This discrepancy can be traced to the z -component in the third term in Eq. (15). The first term when using the frequency Eq. (15) in Eq. (13) contains the z -component of $\mathbf{L}_N \times \mathbf{S}_1$, which is numerically very close to zero for the S-90 model. The second term contains the z -component of $\mathbf{S}_2 \times \mathbf{S}_1$, which is also close to zero. In the third term, we have $(n_{12}S_2)$ and the z -component of $\mathbf{n}_{12} \times \mathbf{S}_1$. Both of these terms grow rapidly near the merger. In particular, the z -component of $\mathbf{n}_{12} \times \mathbf{S}_1$ develops significant noise which terminates the line early. Finally, it is very clear that including terms up to 2PN makes an important difference in improving the matching to the numerical solution.

We have carried out comparisons similar to that in Fig. 2 for all the runs in the *B*- and *S*-series. The results in every case are similar; namely, that the dynamics of $d\mathbf{S}_{1,2}/dt$ are very well approximated by 2PN, and this description only starts breaking down close to the merger.

The most significant variation observed in the $d\mathbf{S}_{1,2}/dt$ dynamics from one S-series run to another was the time at which the merger takes place or, equivalently, the time at which the gravitational radiation emitted reaches its maximum (see Table II). The differences in merger time are due to spin hangup [43] of the merger. Figs. 3-7 show the comparison for a few selected models from the *S*-series. The plots show $d\mathbf{S}/dt$ for both BHs. The left panel shows

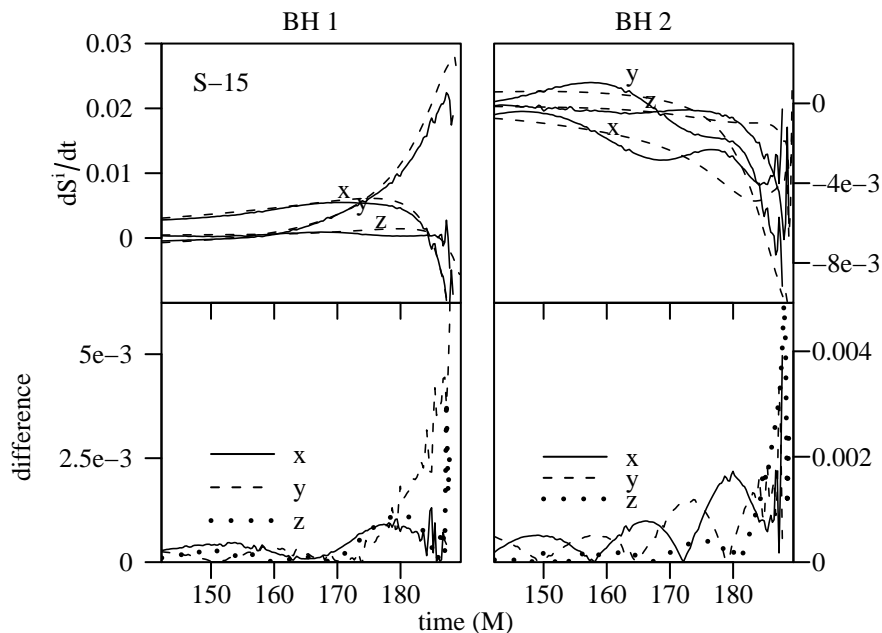


FIG. 3: Comparison of S-15 run numerical to Blanchet 2PN. Left panel shows the results of the comparison for BH₁ and the right panel for BH₂. The top plots on each panel show with a solid line dS^i/dt from our numerical simulations and with a dashed line the values from Blanchet 2PN. The labels denote each component. The bottom plots on each panel show the difference between the numerical solution and the Blanchet 2PN, with solid, dashed and dotted lines for the x , y and z components, respectively.

BH₁, which has the initial spin direction along the negative x -axis. In this case, there is good agreement between the 2PN and computational results for all models. In the right panel, we show BH₂ with a different initial spin direction specified according to the angle θ . For spins of BH₂ more parallel to the orbital angular momentum, the precession becomes smaller (note range of the y -axis to the right of the figure). It seems very likely that with the small precession shown in the S-15 model, the visible disagreement to the PN result is just a numerical artifact that could be cured by higher resolution.

To further understand the spin dynamics, we focus our attention to the evolution of the direction of the spins $\mathbf{S}_{1,2}$ and the vector Σ . Fig. 8 shows the evolution of the spin directional angles $\theta_{1,2}$ and $\varphi_{1,2}$ for the *B-series*. The angles θ and φ are the usual polar and axial angles with respect to the fixed $\{x, y, z\}$ coordinate frame. In all simulations, we found very small changes in the magnitude of the individual spins up to the merger, hence these sky-map plots provide a very good representation of the spin dynamics. The left plot in Fig. 8 shows the individual spins, and the right plot shows the evolution of Σ . All the cases start with $\varphi_1 = -180^\circ$ and $\varphi_2 = 0^\circ$. There are a couple of interesting aspects to notice in Fig. 8. First, there is no significant change in the $\theta_{1,2}$ direction, and hence no change in the θ direction of Σ . Second, in all cases in the *B-series*, the precession is $\Delta\varphi \approx 120^\circ$. Since all the models start with the same $\varphi_{1,2}$, the spin orientation of the BHs arrive at the plunge (the point beyond which most of the kick is accumulated) with the same φ entrance angle. As we shall see in Sec. VI, these two facts, particular to the *B-series*, have an important implication when fitting the gravitational recoils to the Kidder kick formula.

Fig. 9 shows representative evolution tracks of the $\mathbf{S}_{1,2}$ and Σ direction in the θ - φ plane for the *S-series*. The left and central plots in Fig. 9 show the tracks of $\mathbf{S}_{1,2}$ for some of the cases. The left plot includes the $0^\circ \leq \theta = \theta_2 \leq 180^\circ$ models, with the central plot showing the $180^\circ \leq \theta = \theta_2 \leq 360^\circ$ cases. The right plot in Fig. 9 depicts the evolution of Σ for the cases in the left and central plots. All the cases starts out $\varphi_1 = -180^\circ$, $\varphi_2 = 0^\circ$ and $\theta_1 = -90^\circ$. It is clear from Fig. 9 that the spin dynamics are significantly more complicated than in the *B-series* case. A substantial evolution in the θ direction is evident in all cases, and there is also appreciable variation on the rate of φ precession from case to case. There is however a hint of a pattern. The closer the spin of BH₂ aligns or anti-aligns with the z -axis, the larger is the evolution in the θ direction.

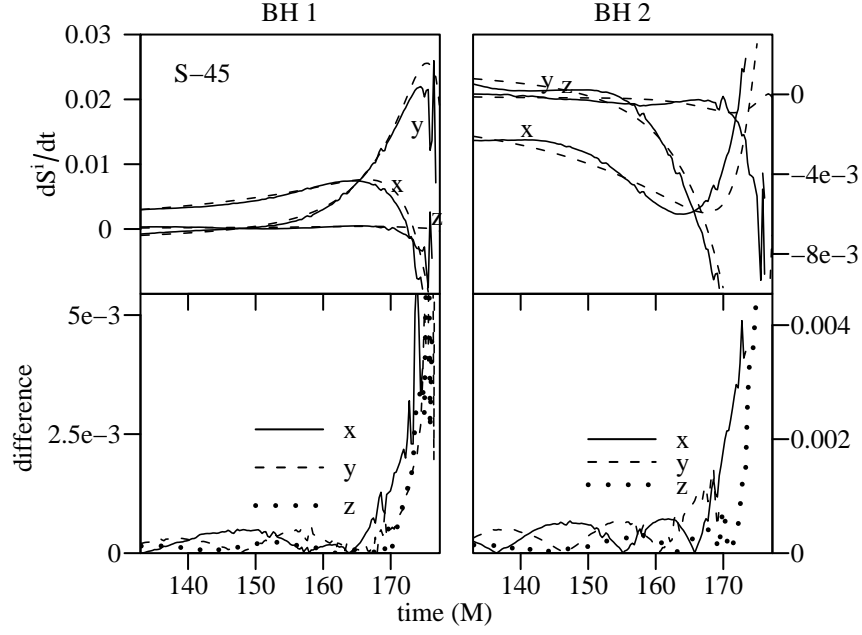


FIG. 4: Same comparison as in Fig. 3 but for the model S-45.

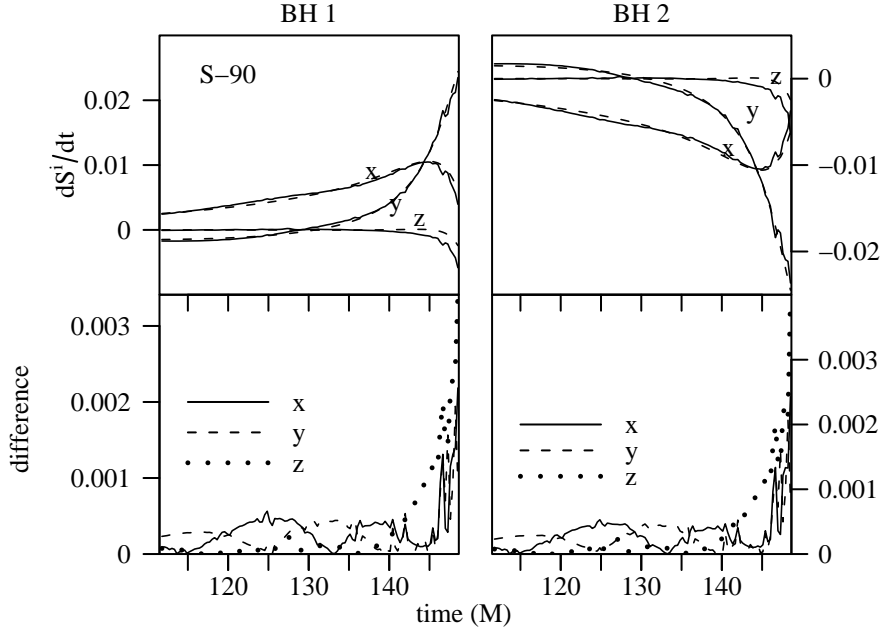


FIG. 5: Same comparison as in Fig. 3 but for the model S-90.

VI. RECOIL ESTIMATES

The gravitational recoil from spinning BHs has been studied for a number of different initial spin configurations [13, 16, 17, 20, 47, 48] including very generic configurations [17] and for a systematic study of variations of the *entrance* angle in the orbital plane (i.e. xy -plane) between the spin vector and the x -axis of anti-aligned BHs in Ref. [20]. Our study explores the recoil of spin orientations out of the xy -plane. Among other things, our aim is to test the assumption implied by the Kidder kick formula Eq. (5) that the recoil velocity can be split into components perpendicular and parallel to the orbital plane that depend on spin entrance angles at the plunge.

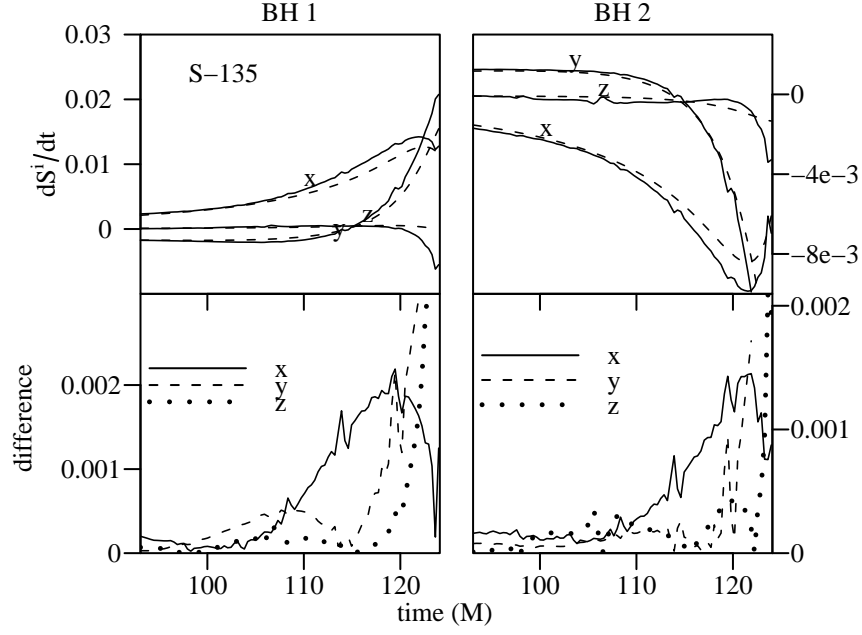


FIG. 6: Same comparison as in Fig. 3 but for the model S-135.

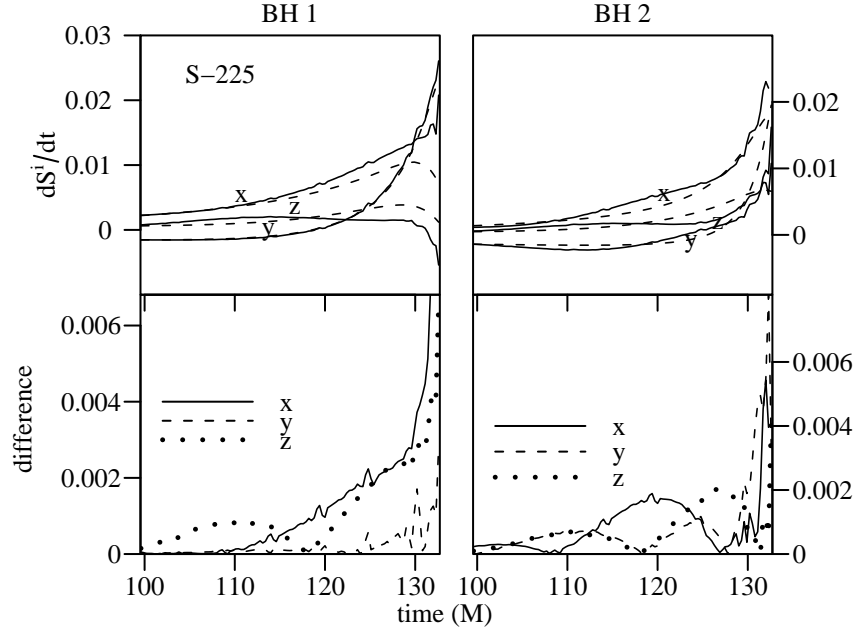


FIG. 7: Same comparison as in Fig. 3 but for the model S-225.

We now specialize the Kidder kick formula to the B-Series. We denote by $\hat{\theta}$ the angle between σ and the orbital angular momentum direction \mathbf{l} . In addition, the angle $\hat{\varphi}$ is the axial angle in the $\mathbf{n-k}$ plane relative to the \mathbf{n} direction. In terms of these angles, the cosine directions in the Kidder kick formula Eq. (5) read:

$$\begin{aligned} (l\sigma) &= \cos \hat{\theta} \\ (n\sigma) &= \sin \hat{\theta} \cos \hat{\varphi} \\ (k\sigma) &= \sin \hat{\theta} \sin \hat{\varphi}. \end{aligned}$$

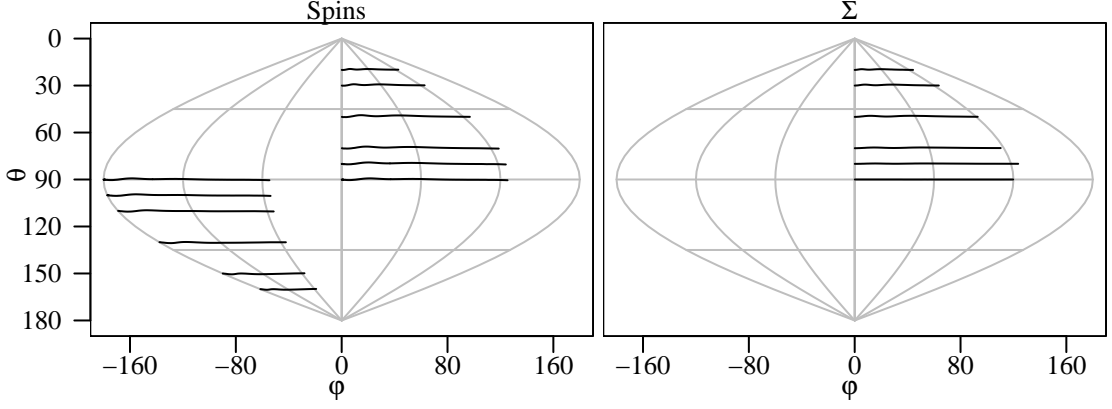


FIG. 8: The evolution tracks of the $\mathbf{S}_{1,2}$ and Σ directions in the θ - φ plane for all the cases in the *B-series*. The left plot shows the individual spins and the right plot shows the evolution of Σ . All the cases start with $\varphi_1 = -180^\circ$ and $\varphi_2 = 0^\circ$. Notice that there is almost no change in the $\theta_{1,2}$ direction for the individual spins or for Σ .

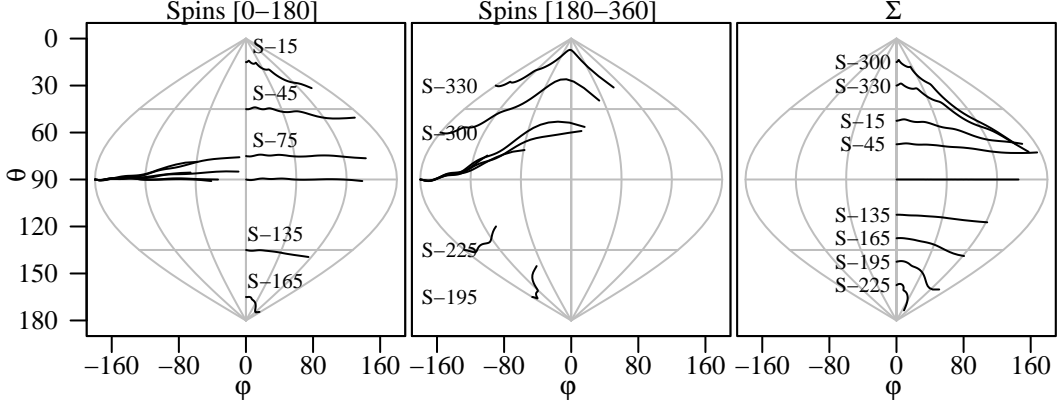


FIG. 9: Representative evolution tracks of the $\mathbf{S}_{1,2}$ and Σ direction in the θ - φ plane for the *S-series*. The left plot shows the tracks of $\mathbf{S}_{1,2}$ for some of the cases in which $0^\circ \leq \theta = \theta_2 \leq 180^\circ$, the central plot for $180^\circ \leq \theta = \theta_2 \leq 360^\circ$ and the right plot the evolution of Σ for the cases in the left and central plots. All the cases start with $\varphi_1 = -180^\circ$, $\varphi_2 = 0^\circ$ and $\theta_1 = -90^\circ$.

For generic cases, the angles $\hat{\theta}$ and $\hat{\varphi}$ are different from the polar angle θ and axial angle φ introduced in Sec. II, which were defined with respect to the fixed $\{x, y, z\}$ coordinate system. This is because the $\{\mathbf{l}, \mathbf{n}, \mathbf{k}\}$ system, by design, is attached to the orbital motion of the binary; hence, it will follow also its precession. However, for all the cases we have considered, to a good approximation, the vector \mathbf{l} stays aligned with the z -axis. Thus, $\hat{\theta} \approx \theta$.

One of the goals of our work is to single out and explore the θ projection dependence. That was the main motivation for constructing the *B-series*. In Sec. V, we saw that for each model in the *B-series* the angles $\theta_{1,2}$ remained fairly constant and the precession was such that the angles $\varphi_{1,2}$ changed by the same amount in all models. As a consequence, it is possible to use φ in the Kidder kick formula and write the kick velocity in terms of the x , y and z -components as:

$$\begin{aligned} V^x &= C_o H_x \cos \theta \\ V^y &= C_o H_y \cos \theta \\ V^z &= C_o K_z \sin \theta \end{aligned} \tag{16}$$

where $C_o = \Sigma q^2 / (M^2(1+q)^4)$ and $K_z \equiv K_k \sin \varphi + K_n \cos \varphi$. H_x and H_y are related to H_n and H_k by a rotation in the xy -plane. Since in our study $q = 1$ and $\Sigma/M^2 = 0.6$, then $C_o = 0.0375$. Notice that $V_{\max}^x = V^x(\theta = 0^\circ) = C_o H_k$, $V_{\max}^y = V^y(\theta = 0^\circ) = C_o H_n$, and $V_{\max}^z = V^z(\theta = 90^\circ) = C_o K$.

Fig. 10 shows the x , y and z -components of the recoil velocity as a function of the initial value of θ for all the cases in the *B-series*. We have also added the $\theta = 0^\circ$ case studied in Ref. [13]. The gravitational recoil was computed from

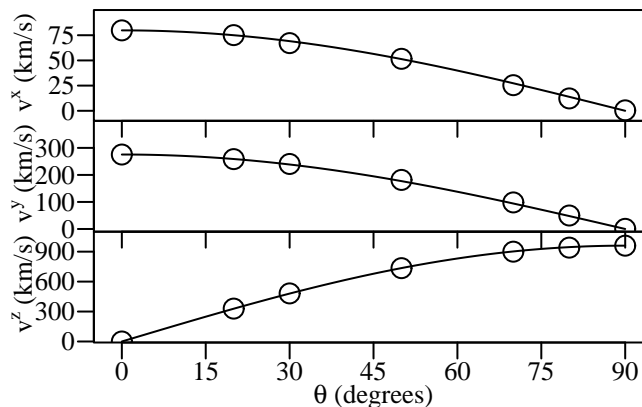


FIG. 10: Recoil velocity components for the *B-series* as a function of the initial angle θ , the angle between Σ and the orbital angular momentum. Circles denote numerical values from the simulations, and the lines are obtained from $V^{(x,y)} = V_{\max}^{(x,y)} \cos \theta$ and $V_{\max}^z \sin(\theta)$, where $V_{\max}^{(x,y)}$ are simply the recoil velocity components obtained for the B-0 and, similarly, V_{\max}^z for the B-90 model.

the Newman-Penrose quantity Ψ_4 at $r/M = \{30, 40, 50, 60\}$. The plot shows $r = 30M$. The results for the other detectors are of similar quality except for $r = 60M$ where the resolution drops. In addition to the recoil data, we also shows the curves $V^{(x,y)} = V_{\max}^{(x,y)} \cos \theta$ and $V_{\max}^z \sin \theta$ where $V_{\max}^{(x,y)}$ are simply the recoil velocity components obtained for the B-0 and, similarly, V_{\max}^z for the B-90 model. We emphasize that no fitting to a $\sin \theta$ or $\cos \theta$ function was done in constructing Fig. 10. Clearly the recoil velocity follows the $\sin \theta$ and $\cos \theta$ curves which is expected from the recoil formulas Eqs. (16) and (11). This was possible because for the *B-series* there is a clear way of measuring the *entrance* angles. We found that $V_{\max}^x = 80 \pm 12$, $V_{\max}^y = 275 \pm 41$ and $V_{\max}^z = 960 \pm 144 \text{ km s}^{-1}$, which yields the constants $H_x = (2.1 \pm 0.3) \cdot 10^4$, $H_y = (7.3 \pm 1) \cdot 10^4$ and $K_z = (2.6 \pm 0.4) \cdot 10^5$.

Because of the complicated dynamics in the *S-series*, we were not able to find a simple method for determining the *entrance* angles. As a consequence, it was not possible to do fittings to the Kidder kick formula. We are currently investigating [49] an approach that explicitly accounts for the precession dynamics that could potentially handling arbitrary configurations.

VII. CONCLUSIONS

The dynamics of BHs in interaction and merger, the gravitational radiation produced and the resulting kick in the final merge BH have direct implementations for understanding a wide range of astrophysical phenomena. These include the development of large scale structure, the structural evolution of galaxies, the detectability (for instance in the detector LISA) of gravitational radiation from the merger, and the statistics of double-nucleus galaxies.

Our work concentrated on investigating the dynamics of spins in BBH systems and the gravitational recoil that the final BH experiences as a result of the merger. Regarding the spin dynamics, we have shown that spin precession follows fairly well the 2PN predictions up to the merger. Although we have only investigated two families of initial orientations (*B-series* and *S-series*), we believe that they represent fairly generic orientations, thus we speculate that the spin dynamics agreement with 2PN will be true for all orientation cases. It remains to be seen whether the agreement deteriorates when relaxing the condition of equal spin-magnitudes and/or masses. Spin-spin PN effects were not found to be significant for the cases we considered.

An interesting aspect of the *B-series*, with BH spins initially anti-aligned with respect to each other, was that for each case the spins precessed about the orbital angular momentum axis, while keeping their polar (θ) angle very closely constant. Also very interesting is that for all the models in the *B-series*, the vector Σ precessed almost the same amount about the orbital angular momentum axis. We were therefore able to read off the *entrance* angles and to demonstrate that the $\sin \theta$ and $\cos \theta$ dependences in the rate of linear momentum radiated as derived in Eq. (11) get directly translated into the Kidder kick formula Eq. (5).

For the *S-series* a more complicated spin dynamics is found and the lack of symmetry between the BHs allows more complicated radiation and kick results in this case. We will continue addressing comparisons to 2PN and the validity of the Kidder kick formula for generic configurations in a separate paper [49].

Acknowledgments

The authors acknowledge the support of the Center for Gravitational Wave Physics funded by the National Science Foundation under Cooperative Agreement PHY-0114375. This work was supported by NSF grants PHY-0354821 to Deirdre Shoemaker, PHY-0244788 and PHY-0555436 to Pablo Laguna and PHY-0354842 and NASA grant NNG 04GL37G to Richard Matzner. Computations were carried out at NCSA under allocation TG-PHY060013N, and at the Texas Advanced Computation Center, University of Texas at Austin.

-
- [1] J. G. Baker, J. Centrella, D.-I. Choi, M. Koppitz, and J. van Meter, Phys. Rev. Lett. **96**, 111102 (2006), gr-qc/0511103.
 - [2] M. Campanelli, C. O. Lousto, P. Marronetti, and Y. Zlochower, Phys. Rev. Lett. **96**, 111101 (2006), gr-qc/0511048.
 - [3] F. Herrmann, I. Hinder, D. Shoemaker, and P. Laguna, Class. Quant. Grav. **24**, S33 (2007).
 - [4] J. G. Baker, J. Centrella, D.-I. Choi, M. Koppitz, J. R. van Meter, and M. C. Miller, Ap. J. Lett. **653**, L93 (2006), astro-ph/0603204.
 - [5] J. A. Gonzalez, U. Sperhake, B. Bruegmann, M. Hannam, and S. Husa, preprint (gr-qc/0610154) (2006).
 - [6] D. Richstone et al., Nature (London) **395**, 14 (1998), astro-ph/9810378.
 - [7] J. Magorrian et al., Astron. J. **115**, 2285 (1998), astro-ph/9708072.
 - [8] Z. Haiman, Astrophys. J. **613**, 36 (2004), astro-ph/0404196.
 - [9] M. Micic, T. Abel, and S. Sigurdsson, preprint (astro-ph/0609443) (2006).
 - [10] P. Madau and E. Quataert, Ap. J. Lett. **606**, L17 (2004), astro-ph/0403295.
 - [11] D. Merritt, M. Milosavljevic, M. Favata, S. A. Hughes, and D. E. Holz, Astrophys. J. **607**, L9 (2004), astro-ph/0402057.
 - [12] K. S. Thorne, Rev. Mod. Phys. **52**, 299 (1980).
 - [13] F. Herrmann, I. Hinder, D. Shoemaker, P. Laguna, and R. A. Matzner, Astrophys. J. **661**, 430 (2007), arXiv:gr-qc/0701143.
 - [14] M. J. Fitchett, Mon. Not. R. astr. Soc. **203**, 1049 (1983).
 - [15] M. J. Fitchett and S. Detweiler, Mon. Not. R. astr. Soc. **211**, 933 (1984).
 - [16] M. Koppitz, D. Pollney, C. Reisswig, L. Rezzolla, J. Thornburg, P. Diener, and E. Schnetter, ArXiv General Relativity and Quantum Cosmology e-prints (2007), gr-qc/0701163.
 - [17] M. Campanelli, C. Lousto, Y. Zlochower, and D. Merritt, Ap. J. Lett. **659**, L5 (2007), arXiv:gr-qc/0701164.
 - [18] L. E. Kidder, Phys. Rev. D **52**, 821 (1995).
 - [19] J. A. Gonzalez, M. D. Hannam, U. Sperhake, B. Brugmann, and S. Husa (2007), gr-qc/0702052.
 - [20] M. Campanelli, C. O. Lousto, Y. Zlochower, and D. Merritt, ArXiv General Relativity and Quantum Cosmology e-prints (2007), gr-qc/0702133.
 - [21] J. G. Baker, W. D. Boggs, J. Centrella, B. J. Kelly, S. T. McWilliams, M. C. Miller, and J. R. van Meter, ArXiv Astrophysics e-prints (2007), astro-ph/0702390.
 - [22] J. D. Schnittman and A. Buonanno, ArXiv Astrophysics e-prints (2007), astro-ph/0702641.
 - [23] G. Faye, L. Blanchet, and A. Buonanno, Phys. Rev. **D74**, 104033 (2006), gr-qc/0605139.
 - [24] T. Nakamura, K. Oohara, and Y. Kojima, Prog. Theor. Phys. Suppl. **90**, 1 (1987).
 - [25] M. Shibata and T. Nakamura, Phys. Rev. D **52**, 5428 (1995).
 - [26] T. W. Baumgarte and S. L. Shapiro, Phys. Rev. D **59**, 024007 (1999), gr-qc/9810065.
 - [27] S. Brandt and B. Brüggmann, Phys. Rev. Lett. **78**, 3606 (1997), gr-qc/9703066.
 - [28] C. Bona, J. Massó, E. Seidel, and J. Stela, Phys. Rev. D **56**, 3405 (1997), gr-qc/9709016.
 - [29] M. Alcubierre, B. Brüggmann, P. Diener, M. Koppitz, D. Pollney, E. Seidel, and R. Takahashi, Phys. Rev. D **67**, 084023 (2003), gr-qc/0206072.
 - [30] J. R. van Meter, J. G. Baker, M. Koppitz, and D.-I. Choi, Phys. Rev. **D73**, 124011 (2006), gr-qc/0605030.
 - [31] M. Hannam, S. Husa, D. Pollney, B. Brugmann, and N. O’Murchadha, preprint (gr-qc/0606099) (2006).
 - [32] B. Bruegmann, J. A. Gonzalez, M. Hannam, S. Husa, U. Sperhake, and W. Tichy, ArXiv General Relativity and Quantum Cosmology e-prints (2006), gr-qc/0610128.
 - [33] S. Husa, I. Hinder, and C. Lechner, Computer Physics Communications **174**, 983 (2006), gr-qc/0404023.
 - [34] Cactus, <http://www.cactuscode.org> (2007).
 - [35] E. Schnetter, S. H. Hawley, and I. Hawke, Class. Quantum Grav. **21**, 1465 (2004), gr-qc/0310042.
 - [36] M. Ansorg, B. Brüggmann, and W. Tichy, Phys. Rev. D **70**, 064011 (2004), gr-qc/0404056.
 - [37] G. B. Cook, Phys. Rev. D **50**, 5025 (1994).
 - [38] T. W. Baumgarte, Phys. Rev. D **62**, 024018 (2000), gr-qc/0004050.
 - [39] M. Campanelli, C. O. Lousto, and Y. Zlochower, preprint (gr-qc/0604012) (2006).
 - [40] O. Dreyer, B. Krishnan, D. Shoemaker, and E. Schnetter, Phys. Rev. D **67**, 024018 (2003), gr-qc/0206008, URL <http://link.aps.org/abstract/PRD/v67/e024018>.
 - [41] A. Ashtekar and B. Krishnan, Living Rev. Rel. **7**, 10 (2004), gr-qc/0407042.
 - [42] E. Schnetter, B. Krishnan, and F. Beyer, Phys. Rev. **D74**, 024028 (2006), gr-qc/0604015.
 - [43] M. Campanelli, C. O. Lousto, Y. Zlochower, B. Krishnan, and D. Merritt, ArXiv General Relativity and Quantum Cosmology e-prints (2006), gr-qc/0612076.

- [44] J. Thornburg, *Class. Quantum Grav.* **21**, 743 (2004), gr-qc/0306056.
- [45] G. B. Cook, *Phys. Rev. D* **50**, 5025 (1994).
- [46] L. Blanchet, A. Buonanno, and G. Faye, *Phys. Rev. D* **74**, 104034 (2006), arXiv:gr-qc/0605140.
- [47] D.-I. Choi, B. J. Kelly, W. D. Boggs, J. G. Baker, J. Centrella, and J. van Meter, *ArXiv General Relativity and Quantum Cosmology e-prints* (2007), gr-qc/0702016.
- [48] W. Tichy and P. Marronetti, *ArXiv General Relativity and Quantum Cosmology e-prints* (2007), gr-qc/0703075.
- [49] F. Herrmann, I. Hinder, D. M. Shoemaker, P. Laguna, and R. A. Matzner (2007), in preparation.

